Role of the Ge surface during the end of range dissolution

S. Boninelli, G. Impellizzeri, A. Alberti, F. Priolo, Fuccio Cristiano, C. Spinella

Role of the Ge surface during the end of range dissolution

S. Boninelli, G. Impellizzeri, A. Alberti, F. Priolo, F. Cristiano et al.

Citation: Appl. Phys. Lett. **101**, 162103 (2012); doi: 10.1063/1.4759031
View online: http://dx.doi.org/10.1063/1.4759031
View Table of Contents: http://apl.aip.org/resource/1/APPLAB/v101/i16
Published by the American Institute of Physics.

Role of the Ge surface during the end of range dissolution

S. Boninelli,[1,a)] G. Impellizzeri,[1] A. Alberti,[2] F. Priolo,[1] F. Cristiano,[3,4] and C. Spinella[2]
[1]*CNR-IMM MATIS and Dipartimento di Fisica e Astronomia, Università di Catania, Via S. Sofia 64, 95123 Catania, Italy*
[2]*CNR-IMM, VIII Strada 5, 95121 Catania, Italy*
[3]*LAAS-CNRS, 7, Avenue du Colonel Roche, F-31400 Toulouse, France*
[4]*Université de Toulouse, LAAS, F-31400 Toulouse, France*

(Received 10 July 2012; accepted 1 October 2012; published online 16 October 2012)

We investigated the structure of end-of-range (EOR) defects in Ge and the role played by the surface during their dissolution caused by annealing. Ge samples were amorphized with Ge^+ ions at two different energies (30 and 100 keV) in order to induce, after solid phase epitaxial regrowth, the formation of EOR band at different depths. High resolution x-ray diffraction and transmission electron microscopy showed that the EOR population consists mainly on small defects and few dislocation loops lying on ⟨001⟩ planes. The deepest EOR defects are more stable during thermal annealing demonstrating the role of the surface during their dissolution. © *2012 American Institute of Physics*. [http://dx.doi.org/10.1063/1.4759031]

Germanium is today considered a good candidate to complement Si in advanced microelectronic devices because of the higher mobility of holes and electrons,[1,2] the compatibility with the Si manufacturing processes, and the higher dopant solubility.[3]

Similarly to Si, a pre-amorphization step, followed by dopant implantation, can be used to reduce the channeling phenomenon so to realize ultra-shallow junctions. However, the subsequent thermal treatments, necessary to re-crystallize the material by solid phase epitaxy (SPE), induce the formation of interstitial-type end-of-range (EOR) defects behind the original amorphous-crystalline interface (a/c).[4,5] These defects evolve during post-SPE thermal annealing, inducing detrimental effects on the diffusion and electrical activation of the dopant. Indeed, Napolitani *et al.*[6] demonstrated that in Ge (as in Si), the dissolution of EOR damage induces a transient enhanced diffusion of B, while Panciera *et al.*[7] showed that Ge self-interstitials, released by EOR defects, are one of the causes of B deactivation.

In literature, the typology and the thermal evolution of EOR defects in Ge is still unclear. Satta *et al.*[8] did not detect by transmission electron microscopy (TEM) any defect in a Ge sample implanted with 1×10^{15} Ge/cm^2 at 100 keV and annealed at 400 °C for 60 s. On the contrary, Panciera *et al.*[7] observed by TEM that EOR defects not only form but also survive after an annealing at 400 °C for 100 s while they completely disappear after 900 s in agreement with results shown by our group.[9] In addition, Hickey *et al.*[10] observed that Ge implanted with 1×10^{15} Si/cm^2 at 1 MeV creates a buried amorphous layer that, upon regrowth, exhibits EOR defects that dissolve only at temperature above 550 °C. The different behavior in all these defects might be due to the different experimental conditions. Indeed, it is well known that in Si, the surface acts as a recombination center for self-interstitials released from the EOR defects[11] while less it is known in Ge. Thus, our aim in this letter is to shed light on the role of the Ge surface on the EOR defects dissolution.

Ge Czochralski wafers, (100)-oriented, *p*-type (with a resistivity higher than 40 Ω·cm) were implanted with a fluence of 2×10^{14} Ge/cm^2 at 30 keV or at 100 keV. The implanted fluence of 2×10^{14} is in both cases above the amorphization threshold.[12] In order to study the thermal evolution of EOR defects, the as-implanted samples were cut into small pieces and were subjected to various thermal treatments in a conventional furnace under a controlled N_2 flux at 340 °C, 370 °C, or 400 °C for 1 h. TEM analyses were performed with a 200 keV 2010 JEOL instrument to investigate the damage induced by the ion-implantation. Plan view (PV) and cross-section (CS) samples were prepared by means of standard preparation with mechanical grinding and ion milling performed in a GATAN-PIPS apparatus at low energy (3 keV Ar) and low incidence angle (7°) to minimize the irradiation damage. High-resolution x-ray diffraction (HR-XRD) measurements were performed by using a D8 Discover Bruker AXS diffractometer equipped with a kα Cu source and a 4 bounce (022) asymmetric Ge monocromator with an instrumental broadening as low as ∼0.005, to study the effect of the implant on the Ge matrix.

The two energies of 30 and 100 keV of the Ge^+ ion implantation where chosen to obtain two different amorphous thicknesses. The 30 keV implant induces the formation of an amorphous layer from the surface down to a depth of ∼20 nm, while the 100 keV implant induces an amorphous layer extending from the surface down to a depth of ∼90 nm, as verified by TEM analyses (not shown). We evaluated by SRIM (stopping and range of ions in matter)[13] simulations the concentrations of excess interstitials created by the two implants below the a/c interface. The estimated values are $\sim 1.7 \times 10^{16}$ cm^{-2} for the 30 keV implanted sample, and $\sim 1.6 \times 10^{16}$ cm^{-2} for the 100 keV implant. Since the excess of interstitials created by the two implants has been evaluated to be the same, we can conclude that any difference on the defect populations is attributed to their distance from the surface. After the ion implantation process, the samples were annealed at 340 °C for 1 h to induce the SPE regrowth.

HR-XRD $\omega - 2\theta$ diffraction patterns were collected around the (004) Ge reciprocal lattice point, and represented as a function of the deviation ($\Delta \mathbf{q_z}$) from the [004] reciprocal

a)Author to whom correspondence should be addressed. Electronic mail: simona.boninelli@ct.infn.it.

lattice vector $\mathbf{q_z}$ ($\mathbf{q_z} = \mathbf{\Delta k}$, where $|k| = 2\pi / \lambda$, $\lambda = 1.5406$ Å). In the reciprocal space, the scan represents a section through the reciprocal lattice point along the direction of $\mathbf{q_z}$ and around the $|\mathbf{q_{z004}}|$ value. The diffraction pattern collected in the sample implanted at 100 keV shows a large diffuse scattering around the Bragg peak position as an effect of the amorphization of the Ge matrix and partially due to the formation of point defects behind the amorphized depth. After annealing at 340 °C, the diffuse scattering contribution due to the amorphization is recovered, whilst the intensity of the radiation diffused at angles higher than the Bragg reflection stays above that of a germanium reference pattern, over a certain angular extent, as shown by the vertical dashed lines in Fig. 1(a). It is well known[14] that the sign of the asymmetry in the diffuse scattering is related to the sign of the displacement field around the defects, and thus to the nature of the defects. Since, in our case, the asymmetry is above the critical angle, it can be concluded[14] that the defects left by the implant after the SPE process are interstitials atoms, in agreement with results present in literature.[4,5] In Fig. 1(b), the excess of diffuse scattering (I_{excess}) with respect to the reference contribution (calculated in the region marked by dashed lines on the right hand side of the peak) is shown in a double logarithmic plot as a function of $|\Delta q_z|$. It has to be noted that the curve has a double slope: in the low values range, the excess of intensity decreases as Δq^{-2} due to the Huang scattering from the lattice atoms near the defects while at higher values it decays roughly as Δq^{-4} due to the Stokes-Wilson scattering.[14] This kind of behaviour, wherein the Huang scattering contribution depends on q^{-2}, is commonly recognised as due to the presence of clusters of interstitial atoms in a crystalline matrix.[14]

TEM analyses were performed on these samples in order to deeply investigate the microscopic structure of the defect population. In Fig. 2, we compared CS bright field TEM images of the sample implanted at 100 keV [Fig. 2(a)] and at 30 keV [Fig. 2(b)] both annealed at 340 °C. In both cases, EOR defects appear behind the original a/c interface. In particular, the sample implanted at 100 keV shows a ~40 nm thick EOR band placed ~90 nm below the surface [Fig. 2(a)]; the sample implanted at 30 keV and re-crystallized shows a much thinner defect band, less than 10 nm in thickness, with very few EOR defects, placed ~30 nm below the surface [Fig. 2(b)]. High resolution (HR) images of two different types of EOR defects are reported in the insets of Fig. 2(a). At the left top, a small cluster with a radius of ~2 nm is reported, whose contrast hinders to resolve its structure. At the right top, a small dislocation loop (DL) with the characteristic "coffee-bean shape" is shown. The fast Fourier transform analysis (not shown) of this HR image reveals that the habit plane of this small DL lies on the {001} plane, parallel to the surface. The evidence of DL with these characteristics in

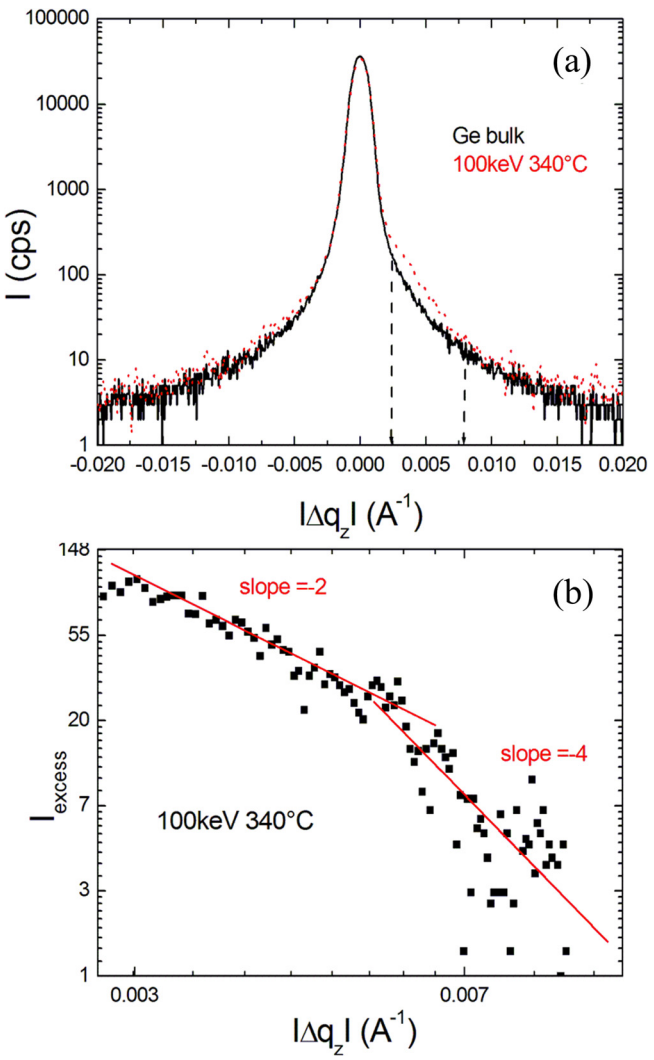

FIG. 1. (a) HR-XR diffraction pattern of the sample implanted at 100 keV and after annealing at 340 °C, compared to that of an unimplanted Ge bulk sample: it has a shoulder at angle above the Bragg one due to diffuse scattering from interstitial-type defects; (b) double log plot of the exceeding intensity, in the region among dashed lines in (a), as a function of $|\Delta q_z|$showing the Huang contribution depending on Δq^{-2}, which indicates the presence of interstitial clusters.

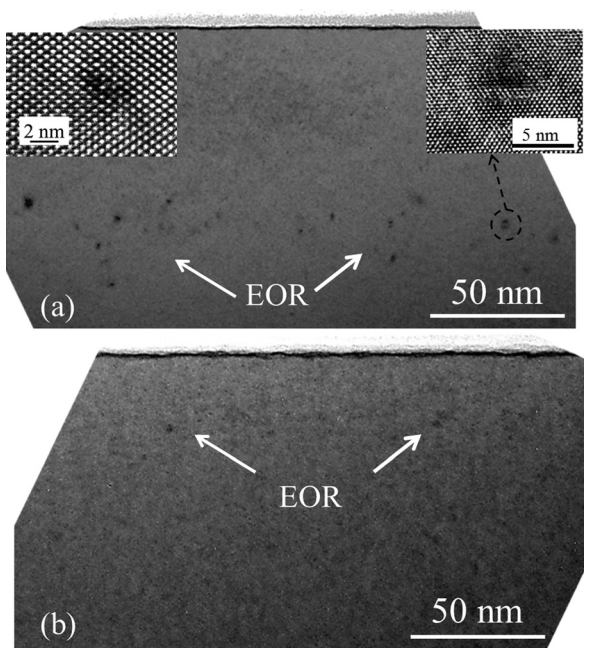

FIG. 2. Cross section TEM of Ge samples implanted with 2×10^{14} Ge/cm^2 at 100 keV (a) and 30 keV (b), after annealing at 340 °C for 1 h. The inset at the left top shows a high resolution image of a small cluster, while the inset at the right top shows a high magnification image of a dislocation loop.

self-implanted Ge is in agreement with similar results reported in literature. Indeed, Hickey *et al.*[10] observed DLs lying on {111} planes (see Fig. 3 of Ref. 10) after high energy amorphizing implants, while Takeda *et al.*[15] detected defects lying on {001} planes after very light ion implantation (deuteron).

To quantitatively estimate the density of the EOR population for different implantation energies and thermal treatments, we analysed the samples by TEM in PV. The EOR defects are usually investigated by TEM in weak beam dark field (WBDF) configuration both in Si[16–18] and Ge,[5,7,10,19] since it allows to visualize the core of the defects with the best contrast. However, since the visibility of each family of defects strongly depends on its crystallographic orientation and on the diffracting **g** vector used for the TEM observation, not all the defect families can be observed in a single image. Thus, a deep knowledge of the defect crystallography is necessary to evaluate the whole defect density. In Si, EOR grow significantly in size during thermal annealing, allowing a better microscopic identification of their structure on the basis of the well-known TEM contrast extinction criteria. Conversely, the EOR defects in Ge generally appear as extremely small clusters (whose size is a few nm) that do not exhibit any direction of elongation, increasing the difficulty of identifying their crystallographic structure. To overcome this limitation, we employed the alternative "zone axis-bright field (ZA-BF)" technique used by Pan *et al.*[20] to visualize all the defects, independently of their atomic structures, although with a lower contrast. In Fig. 3, we compared PV TEM of the samples implanted at 100 keV [Fig. 3(a)] and at 30 keV [Fig. 3(b)] and annealed at 340 °C. It is evident that the density of defects in the sample implanted at 100 keV is higher than that present in the sample implanted at 30 keV. For the quantification of EOR, in terms of mean diameter and areal density, we should take into account that the TEM sample preparation of Ge induces the formation of artifacts, which appear in BF images as small (few nm in diameter) and dark clusters whose contrast and dimensions are similar to those of EOR. This peculiarity of Ge makes the EOR quantification a difficult task. To solve this problem, a virgin Ge TEM sample has been prepared in both CS and PV configuration by identical procedure and treated as a reference (not shown). The analysis of several PV images taken at different magnifications shows that the mean diameter of artifacts is less than 3 nm and their areal density is about $(1.1 \pm 0.2) \times 10^{10}$ artifacts/cm^2, therefore for the real evaluation of the EOR density produced by Ge implantation, we removed these background counts.

The mean diameter, d, and the effective areal density, σ, of the EOR defects are reported in Fig. 4 as a function of the different annealing temperatures and of the different implantation conditions. We found $d = (5 \pm 1)$ nm and $\sigma = (3.3 \pm 0.2) \times 10^{10}$ defects/cm^2 for the sample implanted at 100 keV (square and circle symbols) and $d = (4 \pm 1)$ nm and $\sigma = (0.3 \pm 0.2) \times 10^{10}$ defects/cm^2 for the sample implanted at 30 keV (triangle and stars symbols), both annealed at 340 °C.

Even if the areal density of the 30 keV implanted sample, obtained after the removal of the background, indicates a drastic reduction of the defects density, the mean defect diameter (~4 nm) is higher than that (<3 nm) of artifacts in virgin Ge. The trend is confirmed for the annealing at

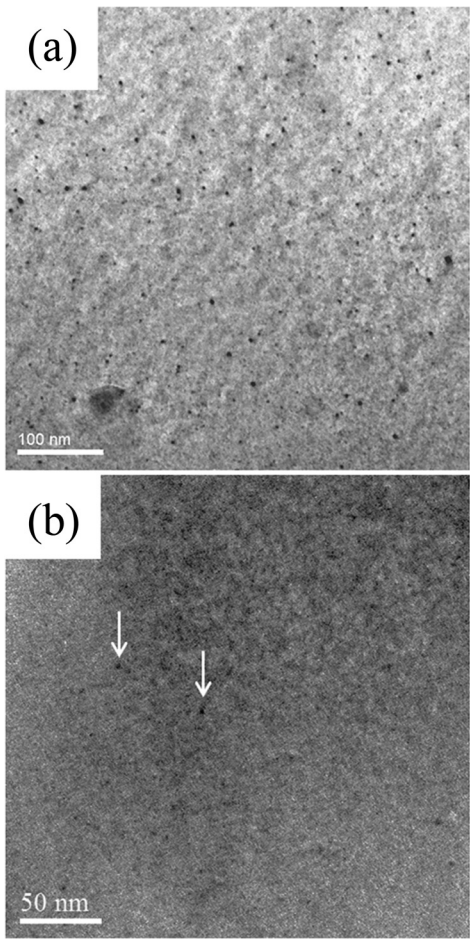

FIG. 3. Plan view TEM images of Ge samples implanted with 2×10^{14} Ge/cm^2 at 100 keV (a) and 30 keV (b), after annealing at 340 °C for 1 h.

370 °C, in fact we measured $d = (4 \pm 1)$ nm and $\sigma = (1.9 \pm 0.2) \times 10^{10}$ defects/cm^2 for the sample implanted at 100 keV and $d < 3$ nm with σ around the background value for the sample implanted at 30 keV, suggesting a complete dissolution of EOR. Finally, we have no evidence of any defect after annealing at 400 °C for sample implanted at 100 keV.

All these results point out some considerations. First of all, the reduction of the EOR density as a function of the thermal budget, for samples implanted at 100 keV, indicates that the defect population tends to shrink and, progressively, to

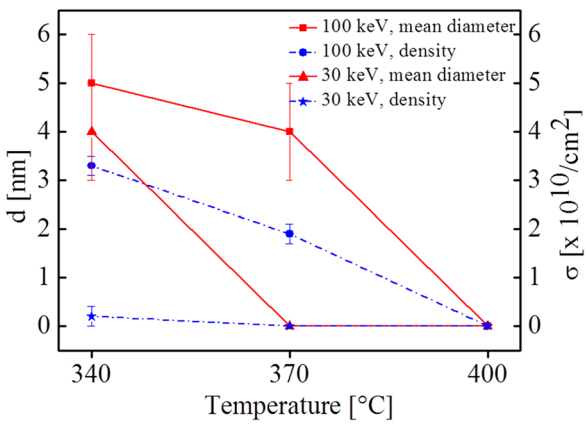

FIG. 4. Evolution of the effective defect mean diameter and the defect density as a function of the temperature.

dissolve. Moreover, the defect density observed at 340 °C for the 30 keV implant [$(0.3 \pm 0.2) \times 10^{10}$ defects/cm^2] is much lower than the one observed in the sample implanted at 100 keV [$(3.3 \pm 0.2) \times 10^{10}$] clearly indicating that the proximity of the surface affects the defect stability. This effect is even more evident if we consider the samples annealed at 370 °C; about 60% of the defects survive for the 100 keV implant [from $(3.3 \pm 0.2) \times 10^{10}$ to $(1.9 \pm 0.2) \times 10^{10}$ defects/cm^2], while all defects dissolve for 30 keV implant. These observations strongly suggest that the Ge surface acts as a sink for self-interstitials.

To better clarify the role of the surface, further studies should be conducted: a vacancies injection from the surface or the presence of dangling bonds at the surface could favor the self-interstitials annihilation, strongly altering the defects density. The large variety of results reported in the literature can be easily exploited on the basis of the different distance between the damage and the surface.

In conclusion, we clearly demonstrated by HR-XRD and TEM analyses that EOR defects in Ge are made mainly of small defects and few dislocation loops lying on ⟨001⟩ planes. After an accurate quantitative analysis that has taken also into account the defects background induced by the TEM sample preparation, we observed that these defects dissolve during thermal annealing with a dissolution rate that strongly depends on their proximity to the surface demonstrating a role of the surface in the recombination of the interstitials.

The authors wish to thank C. Percolla and S. Tatì (CNR-IMM MATIS) for their expert technical assistance. S.B. is grateful to C. Bongiorno (CNR-IMM) for scientific discussions.

[1]S. M. Sze and J. C. Irvin, Solid State Electron. **11**, 599 (1968).
[2]S. Mirabella, G. Impellizzeri, A. M. Piro, E. Bruno, and M. G. Grimaldi, Appl. Phys. Lett. **92**, 251909 (2008).
[3]C. Claeys and E. Simoen, *Germanium-Based Technologies—From Materials to Devices* (Elsevier, Amsterdam, 2007).
[4]G. Bisognin, S. Evangelista, and E. Bruno, Mater. Sci. Eng. B **154–155**, 64 (2008).
[5]S. Koffel, N. Cherkashin, F. Houdellier, M. J. Hytch, G. Benassayag, P. Scheiblin, and A. Claverie, J. Appl. Phys. **105**, 126110 (2009).
[6]E. Napolitani, G. Bisognin, E. Bruno, M. Mastromatteo, G. G. Scapellato, S. Boninelli, D. De Salvador, S. Mirabella, C. Spinella, A. Carnera, and F. Priolo, Appl. Phys. Lett. **96**, 201906 (2010).
[7]F. Panciera, P. F. Fazzini, M. Collet, J. Bedel, and F. Cristiano, Appl. Phys. Lett. **97**, 012105 (2010).
[8]A. Satta, E. Simoen, T. Janssens, T. Clarysse, B. De Jaeger, A. Benedetti, I. Hoflijk, B. Brijs, M. Meuris, and W. Vandervorst, Appl. Phys. Lett. **87**, 172109 (2005).
[9]S. Boninelli, G. Impellizzeri, F. Priolo, E. Napolitani, and C. Spinella, Nucl. Instrum. Methods B **282**, 21 (2012).
[10]D. P. Hickey, Z. L. Bryan, K. S. Jones, R. G. Elliman, and E. E. Haller, Appl. Phys. Lett. **90**, 132114 (2007).
[11]D. R. Lim, C. S. Rafferty, and F. P. Klemens, Appl. Phys. Lett. **67**, 2302 (1995).
[12]G. Impellizzeri, S. Mirabella, and M. G. Grimaldi, Appl. Phys. A **103**, 323 (2011).
[13]J. F. Ziegler, Nucl. Instrum. Methods B **219–220**, 1027 (2004).
[14]P. H. Dederichs, J. Phys. F: Metal Phys. **3**, 471 (1973).
[15]S. Takeda, *Inst. Phys. Conf. Ser.* (IOP Publishing Ltd, 1997), Vol. 157.
[16]J. Li and K. Jones, Appl. Phys. Lett. **73**, 3748 (1998).
[17]A. Claverie, B. Colombeau, B. de Mauduit, C. Bonafos, X. Hebras, G. Ben Assayag, and F. Cristiano. Appl. Phys. A **76**, 1025 (2003).
[18]S. Boninelli, N. Cherkashin, A. Claverie, and F. Cristiano, Appl. Phys. Lett. **89**, 161904 (2006).
[19]R. Crosby, K. S. Jones, M. E. Law, A. Nylandsted Larsen, and J. Lundsgaard Hansen, J. Vac. Sci. Technol. B **22**, 1 (2004).
[20]G. Z. Pan, K. N. Tu, and A. Prussin, Appl. Phys. Lett. **68**, 1654 (1996).